Graphene Blisters with Switchable Shapes Controlled by Pressure and Adhesion

Narasimha G. Boddeti[1], Xinghui Liu[1], Rong Long[1, 2], Jianliang Xiao[1], J. Scott Bunch[1], and Martin L. Dunn[3]

[1]Department of Mechanical Engineering, University of Colorado, Boulder, Colorado 80309, United States

[2]Department of Mechanical Engineering, University of Alberta, Edmonton, Alberta T6G 2G8, Canada

[3]Singapore University of Technology and Design, Singapore, 138682

1. Device Fabrication

Suspended graphene membranes were fabricated by a combination of standard micro-fabrication techniques and mechanical exfoliation of graphene. An array of annular cavities with designed dimensions was first patterned by photolithography on a silicon wafer with a layer of 90 nm thick silicon oxide grown by thermal oxidation. The annular rings were further dry-etched down into silicon substrate with about 110 nm depth by reactive ion etching (RIE). After etching, the chips were cleaned with acetone and isopropanol followed by further cleaning in a Nanostrip bath at 60°C for 20 minutes. Finally, suspended graphene membranes were mechanically exfoliated using the Scotch tape method over the annular micro-cavities.

2. Determination of Graphene Thickness

We used a combination of Raman spectroscopy and optical contrast to determine the number of graphene layers. Raman spectroscopy uses Raman (inelastic) scattering of monochromatic light to investigate rotation and vibrational modes in a system. We used the relative integrated intensity of the graphene G peak and the Silicon optical phonon peak, *I(G)/I(Si)* as described in Koh et al[1] to count the number of layers. Figure 1 shows the locations where the Raman spectrum is measured on the monolayer and multi-layered flakes used in the experiment using black and green dots respectively. The plot on the right shows the recorded Raman spectrum with the Si, G and 2D peaks identified. For reference, the Raman spectrum is also measured on a graphene flake with 1-5 layers of graphene identified optically. The recorded spectrum and the

flake with the spots, where the spectrum is measured identified, is as shown in Fig. 2. The relative integrated intensity *I(G)/I(Si)* is plotted in Fig. 3 and as expected it varies linearly with the number of layers. The blue circular dots are from the reference flake and the red triangular dots are from the experimental flakes.

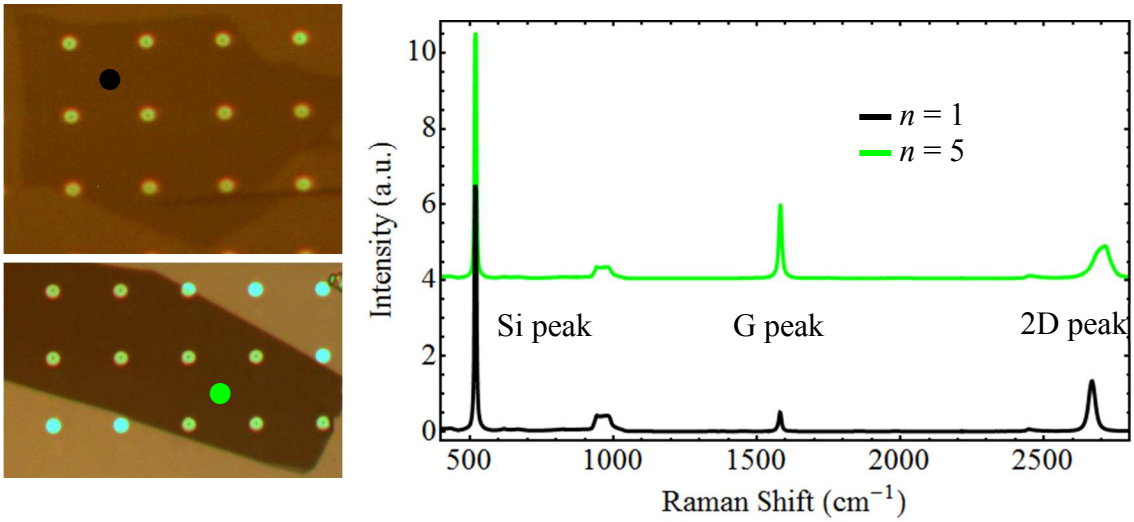

Figure 1 Raman spectroscope of the graphene flakes (optical images on the left) used in the experiment - monolayer (black) and multilayer (green) graphene. The top image on the left is that of monolayer and the bottom one is that of multi-layered graphene. The location where the Raman spectroscopy is done is denoted by black and green dots respectively.

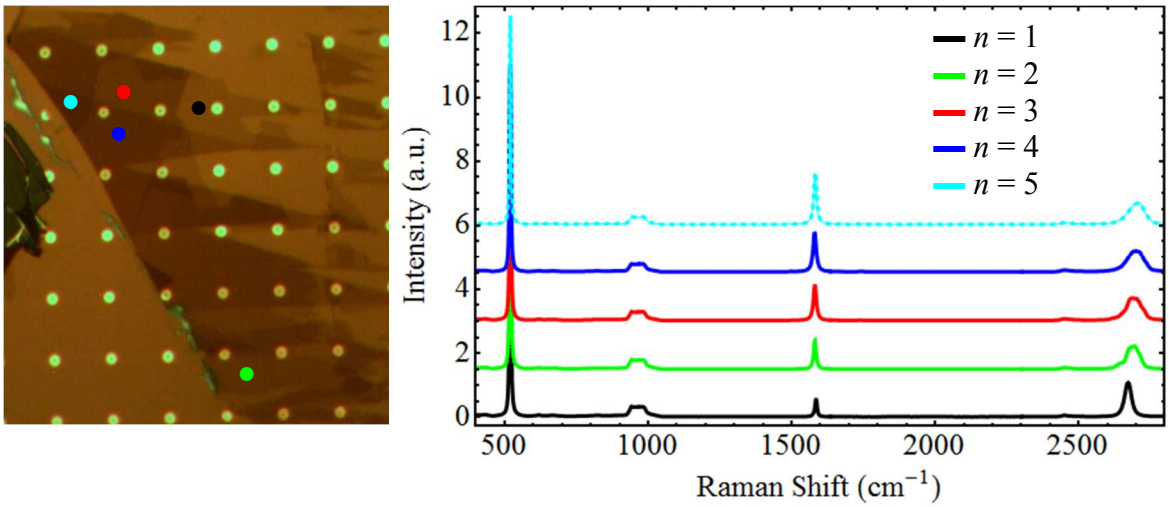

Figure 2 Raman spectroscope of a graphene flake with 1 to 5 layers (n=1 – black, n=2 – green, n=3 – red, n=4 – blue, n=5 – cyan with the solid plot for this flake and the dashed plot for the experimental flake) used to confirm the number of layers in the multilayer graphene flake.

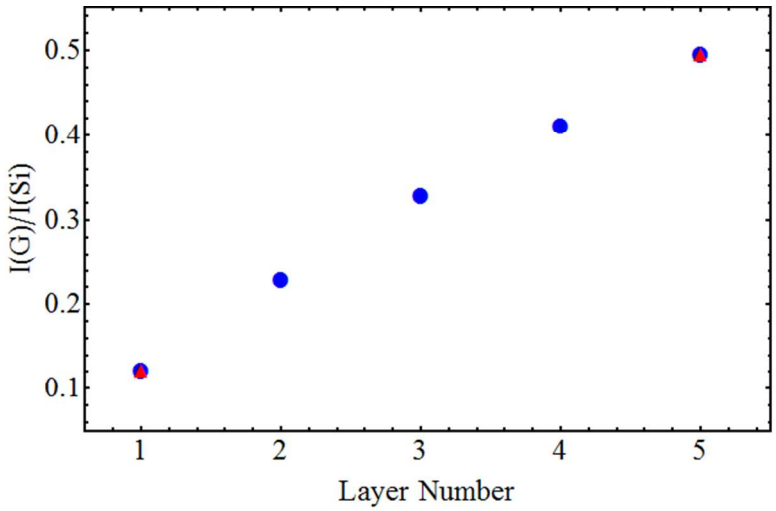

Figure 3 Integrated intensities, I(G)/I(Si) for differently thick graphene sheets. The blue dots are for the graphene in the reference flake and the red triangles are for the sheets that make up the experimental flakes.

3. Mechanics of the Annular Blister Configurations

The mechanics of the annular shaped axisymmetric deformation with the membrane adhered and thereby fixed at $r = a$ and $r = b$, is described by the equation:

$$\frac{d}{dr}\left(rS\frac{dw}{dr}\right) = pr \tag{1}$$

Here r is the radial coordinate, w is the deflection, p is the pressure load across the membrane and S is the membrane stress in the radial direction. With S also being a function of r along with w, there are no known general analytical solutions to eq. (1) with the current boundary conditions to our knowledge[2,3]. To obtain an approximate solution, it is assumed that tangential strain ϵ_t is negligible following Saif et al[4] and that the radial tension S is uniform. This greatly simplifies eq. (1) and after integration, we obtain:

$$w = \frac{pr^2}{4S} + c_1 \ln[r] + c_2 \tag{2}$$

The integration constants c_1 and c_2 can be determined using the boundary conditions at $r = a$ and $r = b$, thus giving:

$$w = \frac{p}{4S}\left((a^2 - r^2) + r_0^2 \ln\left[\frac{r}{a}\right]\right)$$
$$r_0^2 = \frac{a^2 - b^2}{\ln[a/b]} \tag{3}$$

The negative sign is ignored so as to align the deformation along positive direction. Now that we have the deflection profile, the maximum deflection (H) can be obtained by solving $dw/dr = 0$. Equation (4) describes the relationship between maximum deflection H and the load p.

$$H = \frac{p}{4S}\left(a^2 - \frac{r_0^2}{2} + \frac{r_0^2}{2}\ln\left[\frac{r_0^2}{2a^2}\right]\right) \tag{4}$$

The volume occupied by the deformed membrane is given by:

$$V_a = \int_b^a w\, 2\pi r dr = \frac{\pi}{2}\frac{p}{4S}(a^2 - b^2)(a^2 + b^2 - r_0^2) \tag{5}$$

The radial membrane stress, S is still an unknown; it can be obtained from the average radial strain, $\bar{\epsilon_r}$. Assuming the slope $w' = dw/dr$ to be small, we have:

$$\begin{aligned} \bar{\epsilon_r} &= \frac{1}{\pi(a^2 - b^2)}\int_b^a \sqrt{1 + w'^2}\, 2\pi r dr \; - \; 1 \\ &\approx \frac{1}{\pi(a^2 - b^2}\int_b^a \frac{w'^2}{2}\, 2\pi r dr = \frac{S(1 - \nu^2)}{Et} \end{aligned} \tag{6}$$

Completing the integration, we get:

$$S = \left(\frac{Et\, p^2}{16(1 - \nu^2)}(a^2 + b^2 - r_0^2)\right)^{\frac{1}{3}} \tag{7}$$

4. Finite Element Simulations

We assumed that the tangential strain (ϵ_t) is zero and used averaged radial strain (ϵ_r) to obtain an average measure for radial membrane stress (S). While our analysis follows that of Saif et al closely, they averaged the strain along the diameter whereas we averaged it over the entire area of the membrane. Williams[5] assumed equi-biaxial strain condition and obtained an areal average for the total strain – radial and tangential combined. The pressure-displacement relation obtained by us is:

$$H = \left(\frac{p(1 - \nu^2)}{4Et}\right)^{\frac{1}{3}}\left(a^2 - \frac{r_0^2}{2} + \frac{r_0^2}{2}\ln\left[\frac{r_0^2}{2}\right]\right)(a^2 + b^2 - r_0^2)^{-\frac{1}{3}} \tag{8}$$

The expression obtained by Saif et al's approach is –

$$H = \left(\frac{p(1 - \nu^2)}{8Et}\right)^{\frac{1}{3}}\left(a^2 - \frac{r_0^2}{2} + \frac{r_0^2}{2}\ln\left[\frac{r_0^2}{2}\right]\right)\left(\frac{a^2 + b^2 + ab}{3} + \frac{r_0^4}{4ab} - r_0^2\right)^{-\frac{1}{3}} \tag{9}$$

Finally the expression obtained Williams is:

$$H = \left(\frac{p(1-\nu)}{2Et}\right)^{\frac{1}{3}} \left(a^2 - \frac{r_0^2}{2} + \frac{r_0^2}{2}\ln\left[\frac{r_0^2}{2}\right]\right)(a^2 + b^2 - r_0^2)^{-\frac{1}{3}} \quad (10)$$

To determine which of the three above mentioned approaches give the best approximation we carried out finite element simulations, the details of which follow. We used an axisymmetric model with two different geometries - a = 2 μm and b = 0.5 or 1 μm. Two noded axisymmetric shell elements (SAX) with thickness 0.34 nm are used to mesh the membrane to account for both bending and stretching of the membrane. Values of E = 1 TPa and ν = 0.16 are used for material elastic properties which correspond to those of graphene. The "pressure load versus maximum displacement" results from the simulations along with the expressions in eqs. (8), (9) and (10) are plotted in Fig. 4.

The overall load versus deflection response matches quite closely with our analytical expression. The figure 5a shows the deflection profile from our analysis (dashed curves) compared with the FE results at p = 2.51 MPa. We have a reasonably good description of the deflection profile from the theory, even though the radius at which the maximum deflection occurs is not in very good agreement with the FE results. The figures 5b and 5c show the stresses as obtained from the FE simulations at p = 2.51 MPa for the two different geometries ((b) b = 1 μm and (c) b = 0.5 μm). The average radial stress values in each case as calculated from the analysis are 13.29 GPa and 17.54 GPa respectively and are also shown as dashed lines. They are in good agreement with the averaged values for radial stresses calculated from the simulations – 13.24 GPa and 17.04 GPa respectively. The tangential stresses are also in good agreement and consistent with our assumption that the tangential strain is negligible. Also it is to be noted that the residual stress found in graphene membranes is usually of the order of 0.30 GPa which is small compared to the radial stresses we have here at about p = 2 MPa, thereby allowing us to neglect its effect. Even at p = 100 kPa, from eq. (7) the average radial stress is 1.55 GPa, which is still 5 times the typical values of residual stress in graphene.

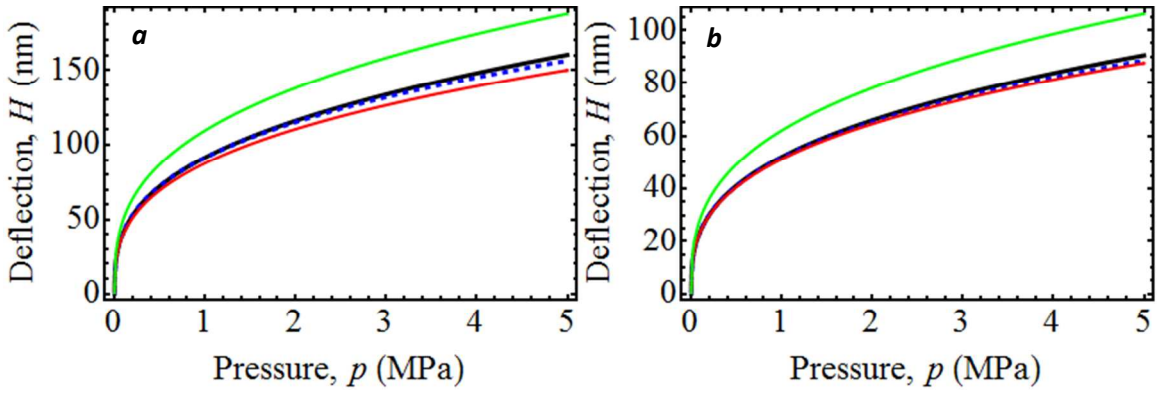

Figure 4 Comparison of the FE simulation results (blue) through the load versus maximum deflection plots with the different analytical expressions - current analysis (eq. (8), dashed), Saif et al's result (eq. (9), red), Williams' result (eq. (10), green) with Et = 340 N/m and ν = 0.16 for two different geometries (a) a = 2 μm, b = 1 μm and (b) a = 2 μm, b = 0.5 μm.

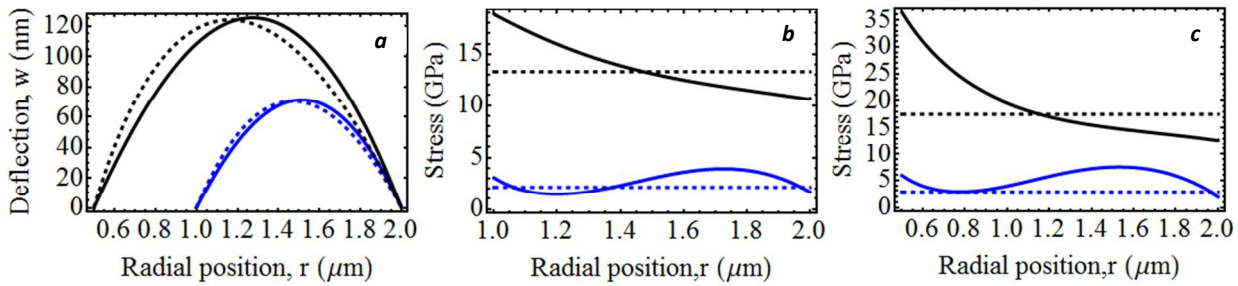

Figure 5 (a) Plots comparing the deflection profile at $p \approx 2.51$ MPa as obtained from the analysis (eq. (3)) and FE (a = 2 μm, Blue – b = 1 μm, Black – b = 0.5 μm, Solid – FE, Dashed – Current Analysis), (b,c) Radial and Tangential stresses in black and blue colored solid curves respectively at $p \approx 2.51$ MPa along the radius of the membrane with a = 2 μm and (b) b = 1 μm, (c) b = 0.5 μm. The black and blue dashed lines are the averaged radial and tangential stresses respectively calculated using the current analysis.

5. Free Energy Contributions

Here we describe in detail how we arrive at eq. (3) in the main text. We stated in the main text that the total free energy, F is the sum of elastic strain energy in the membrane (F_{mem}), free energy associated with isothermal expansion of the fixed mass of gas molecules (F_{gas}), adhesion energy (F_{adh}) and the free energy associated with the external environment.

$$F = F_{mem} + F_{gas} + F_{adh} + F_{ext} \tag{11}$$

The membrane free energy, F_{mem} is the elastic strain energy stored as it deforms when subjected to a pressure difference across it of $p = p_i - p_e$ where p_i is the pressure in the chamber. For any fixed values of radii a and b, we can compute F_{mem} by equating it to the work done by the quasi-statically expanding gas in the cavity and using eqs. (4) and (5):

$$F_{mem} = \int p dV_a \Big|_{a,b} = \frac{pV_a}{4} \tag{12}$$

For specified blister radii, eq. (4) provides a relationship between p, H, a and b; through eq. (5) the volume (V_a) and radii (a and b) are related to the maximum height of the island blister, H. The free energy change due to gas expansion in the cavity with a fixed number of molecules is:

$$F_{gas} = -\int p dV = -p_0 V_0 \ln\left[\frac{V_0 + V_a}{V_0}\right] \tag{13}$$

where $V_0 = \pi h(a_0^2 - b_0^2)$ is the initial volume of the gas i.e. the volume of the micro-cavity with h being the depth of the cavity. The adhesion energy is simply:

$$F_{adh} = \Gamma\pi(a^2 - a_0^2) + \Gamma\pi(b_0^2 - b^2) \tag{14}$$

As the blister expands by V_a, the volume of the surrounding atmosphere decreases by an equal amount V_a (assuming no volume change of the membrane) and thus the free energy of the surrounding pressure reservoir changes by:

$$F_{ext} = p_e V_a \tag{15}$$

Addition of these free energy contributions gives eq. (3) in the main text:

$$F(a,b) = \frac{pV_a}{4} - p_0 V_0 \ln\left[\frac{V_0 + V_a}{V_0}\right] + p_e V_a + \Gamma\pi(a^2 - a_0^2) + \Gamma\pi(b_0^2 - b^2) \tag{16}$$

6. Stability of the Constant N Island Blister Growth

In the main text, we concluded that delamination is favored on the island but not on the outer boundary when the adhesion energies are the same. Hence the only free parameter in the free energy now is the inner radius b:

$$F(b) = \frac{p(b)V_a(b)}{4} - p_0 V_0 \ln\left[\frac{V_0 + V_a(b)}{V_0}\right] + p_e V_a(b) + \Gamma\pi(b_0^2 - b^2) \tag{17}$$

Here, $p = p_i - p_e$ is related to the inner radius via the following equation where $r_0^2 = (a_0^2 - b^2)/\ln[a_0/b]$:

$$\left(\frac{p_0 - p_i}{p_i}\right)^3 V_0^3 = \frac{\pi^3(1-\nu^2)}{32Et}(a_0^2 - b^2)^3(\, a_0^2 + b^2 - r_0^2)^2(p_i - p_e) \tag{18}$$

The equilibrium configuration is obtained by finding the extrema of the free energy i.e. $dF/db = 0$ which gives:

$$\Gamma = \frac{p(b)}{8}\left(\frac{p(b)(1-\nu^2)}{4Et}\right)^{\frac{1}{3}} \frac{5b^4 + a_0^2 b^2 - 5b^2 r_0^2 + r_0^4}{b^2(a_0^2 + b^2 - r_0^2)^{\frac{1}{3}}} \tag{19}$$

Putting $b = b_0$ in (19) gives the critical charging pressure at which delamination begins. Due to the intractable nature of the algebra of showing explicitly the stability or instability of the constant N island blister growth, we use numerical examples to show the same. We start with a system which is close to our experimental geometry with $a_0 = 2\,\mu m$, $b_0 = 0.5\,\mu m$ and $d = 0.2\,\mu m$. Assuming the adhesion energy on the island is $\Gamma = 0.2\,J/m^2$ and using monolayer graphene's material properties ($Et = 340N/m$ and $\nu = 0.16$), the critical charging pressure is 1.39 MPa. The free energies with $F(b_0)$ as the reference are plotted in Fig. 6 at the critical charging pressure load of 1.30 MPa as well as two other pressures each of which are below and above the critical charging pressure.

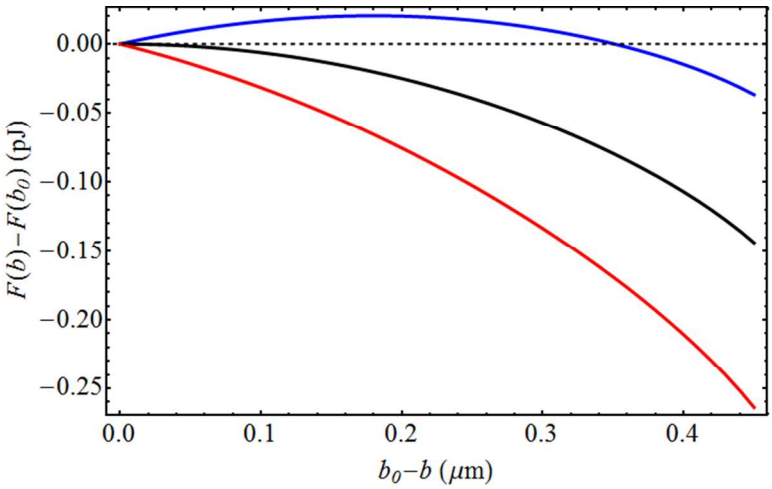

Figure 6 Free energy of the constant N island blister system, $F(b)$ at the critical charging pressure, $p_0 = 1.39\ MPa$ (Black curve) for $a_0 = 2\ \mu m, b_0 = 0.5\ \mu m, d = 0.2\ \mu m$. The blue and red curves are at $p_0 = 1\ MPa$ and $p_0 = 1.8\ MPa$ respectively.

At p_0 = 1 MPa, the system clearly has an energy barrier and thus there will be no delamination. But as p_0 is increased to 1.39 MPa the barrier vanishes and we have a local maximum at $b = b_0$ leading to unstable delamination of the membrane from the island. Beyond the critical charging pressure, there is no energy barrier and the system has a favorable gradient for delamination.

Now let us look at a system where $b_0 = 1.8\,\mu m$ and $d = 0.02\,\mu m$ while the rest of the parameters are the same as mentioned in the previous example. The critical charging pressure obtained from eq. (19) is 17.74 MPa. The free energy is again plotted as a function of the island blister radius in Fig. 7. In this case, as in the previous case, we have a local maximum at $b = b_0$ at the critical charging pressure but we also have an additional maximum and a minimum in between the two maxima. Hence the delamination will be stable due to the presence of the minimum but as the charging pressure is increased, the minimum and maximum come closer and coincide and at this pressure again the delamination will be unstable. It can be seen by the trend in the black and red curves in Fig. 7 how the minimum and maximum come closer. Hence the delamination will be stable only for a specific range of pressures.

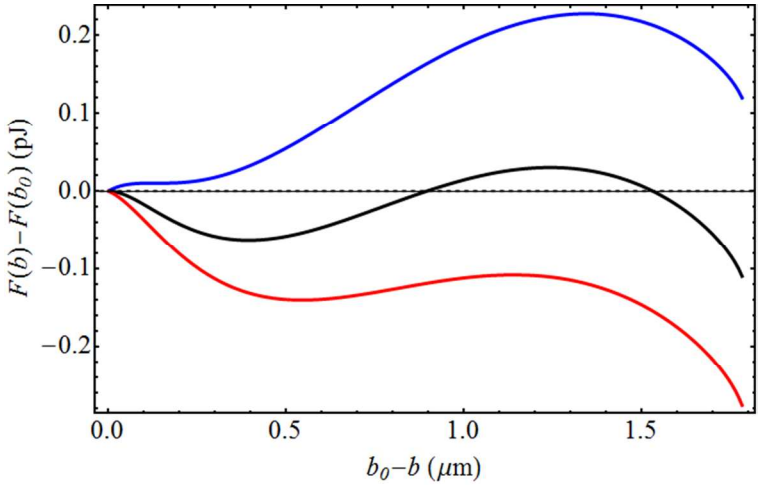

Figure 7 Free energy of the system with $a_0 = 2\ \mu m, b_0 = 1.8\ \mu m, d = 0.02\ \mu m$ *at charging pressures 16 MPa (Blue), 17.74 MPa (Black) and 19 MPa (Red) respectively.*

Now if in the previous case the depth of the cavity is changed to $0.01\ \mu m$ keeping everything else the same, we see a different behavior from the system as shown in Fig. 8. The free energy in this case has a minimum at the critical charging pressure (= 23.32 MPa) at $b = b_0$ meaning the delamination off of the island will be stable. But as in the previous case, the minimum vanishes at a specific charging pressure again resulting in unstable delamination.

In summary, the constant N island blister delamination is unstable for most geometries but can be made stable for a given outer diameter by decreasing the depth of the cavity and increasing the radius of the island. This in effect decreases the initial volume occupied by the pressurized gas. Mathematically speaking, the delamination is unstable because the stiffness of the membrane as it delaminates decreases at a larger rate than the pressure of the expanding gas. But having a large inner radius b and small initial volume can reverse this trend, albeit only for a specific range of pressures.

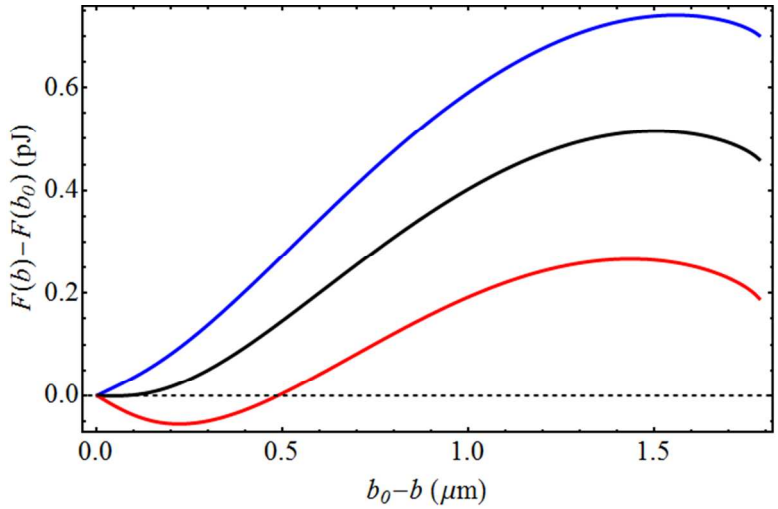

Figure 8 Free energy of the system with $a_0 = 2\ \mu m, b_0 = 1.8\ \mu m, d = 0.01\ \mu m$ *at charging pressures 20 MPa (Blue), 23.32 MPa (Black) and 27 MPa (Red) respectively.*

Figures 9 and 10 show the variation of various critical charging pressures with respect to the system parameters a_0, b_0, d and Γ. We plotted here the critical charging pressures for delamination to occur from outside, delamination from the island and delamination if we have a spherical bulge (instead of annular bulge) in black, blue and red respectively. For Fig. 9, we used parameters $Et = 340\ N/m$, $\nu = 0.16$, $a_0 = 2\ \mu m$, $b_0 = 0.5\ \mu m$, $d = 0.2\ \mu m$ and $\Gamma = 0.2\ J/m^2$ when not being varied. It is clear that delamination pressure from the outer boundary is always larger compared to the delamination pressure from the island in line with our conclusion in the main text. The interesting aspect to be observed here is that there is a critical inner radius (outer radius) above (below) which the critical delamination charging pressure for the island is higher than the critical charging pressure for the spherical blister. This implies that as soon as the

membrane delaminates from the island and forms a spherical blister, it starts to delaminate in the outward direction too.

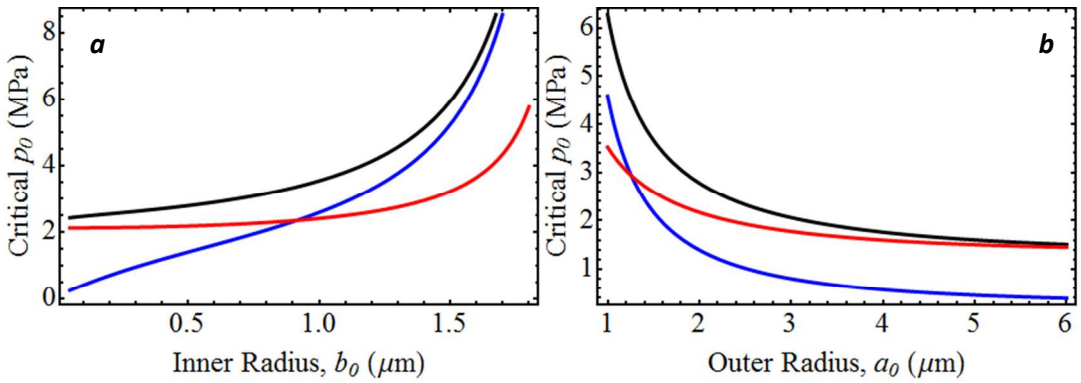

Figure 9 Variation of critical charging pressures with inner radius b_0 *and outer radius* a_0*. When not varied, the values of the other parameters are* $Et = 340\ N/m$, $\nu = 0.16$, $a_0 = 2\ \mu m$, $b_0 = 0.5\ \mu m$, $d = 0.2\ \mu m$ *and* $\Gamma = 0.2\ J/m^2$.

In Fig. 10, we show similar results but we vary the depth of the cavity and the adhesion strength on the island here. The system parameter used in these plots are the same as in Fig. 9 except $b_0 = 1.5\ \mu m$ here. The variation in the depth of the cavity gives a result which looks similar to the results in Fig. 9. When the adhesion strength on the island (Fig. 10b) is varied assuming the adhesion strength on the outer boundary is still $0.2\ J/m^2$, there is a critical adhesion strength at which delamination off of the outer boundary is favored over island delamination. In other words, as we increase the adhesion strength on the island there is a critical value above which the energy release rate for island delamination goes below that for delamination from outer boundary.

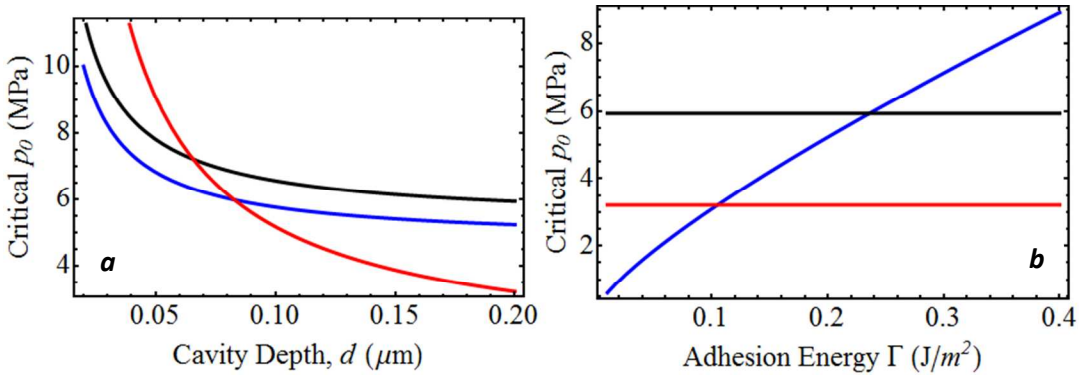

Figure 10 Variation of critical charging pressures with cavity depth d *and island adhesion energy* Γ*. When not varied, the values of the other parameters are* $Et = 340\ N/m$, $\nu = 0.16$, $a_0 = 2\ \mu m$, $b_0 = 1.5\ \mu m$, $d = 0.2\ \mu m$ *and* $\Gamma = 0.2\ J/m^2$.

7. AFM Height Scans of a Monolayer Device

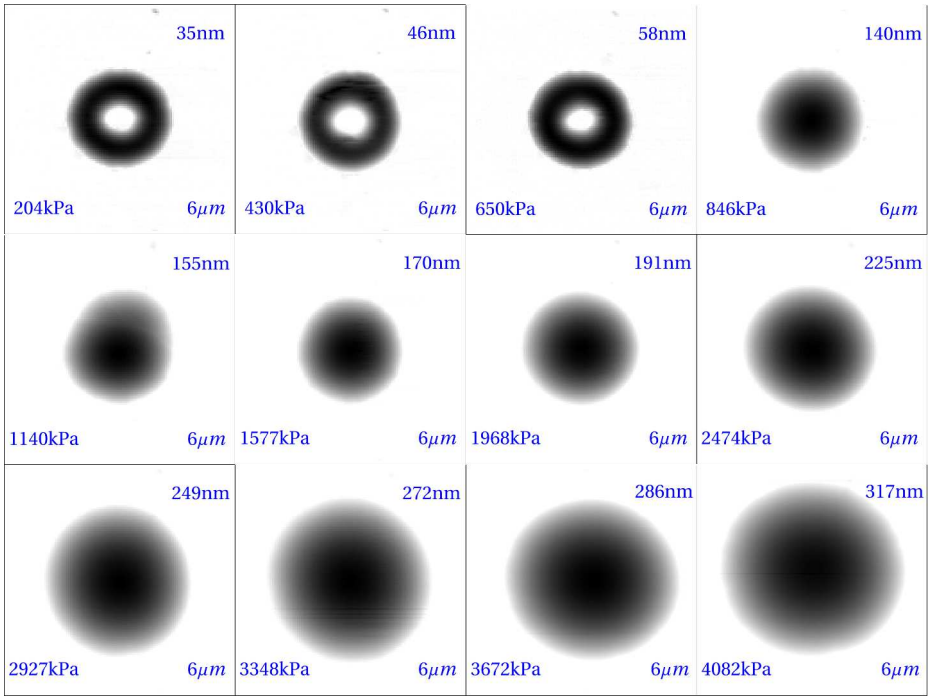

Figure 11 Full AFM Height Scans of a monolayer device arranged in increasing order of charging pressures left to right and top to bottom. Darker regions indicate deflected membrane, while the white region is the graphene adhered to the substrate which is also the reference plane.

8. Sliding of Graphene Membranes

Hencky's series solution[5,6] for clamped/fixed circular membranes describes the mechanics with two constants C_1 and C_2. Since the interfacial shear strength of graphene-SiO_x is finite and if it is small enough, the graphene membrane can slide on the substrate while still being adhered to the substrate[7]. This condition will lead to a larger membrane deflection than that predicted by Hencky's solution. We modified Hencky's solution to reflect the sliding boundary condition, and it turns out that the functional form of the solution remains the same except C_1 and C_2 are now different. We can show that even if C_1 is increased by 10% from the value obtained from Hencky's solution (0.525), the resulting increase in the calculated averaged adhesion energy is only about 3.4%. Hence, for simplicity we kept C_1 = 0.525 and used the resulting value of adhesion energy, 0.160 J/m^2. We then use C_2 as the lone fitting parameter to make the experimental observations (δ, a and p_i) self-consistent. We obtain a value of 0.755 that fits the theory with the experimental observations. This value is 10% higher than the value from Hencky's solution. Figure 12 below shows the results of the fit.

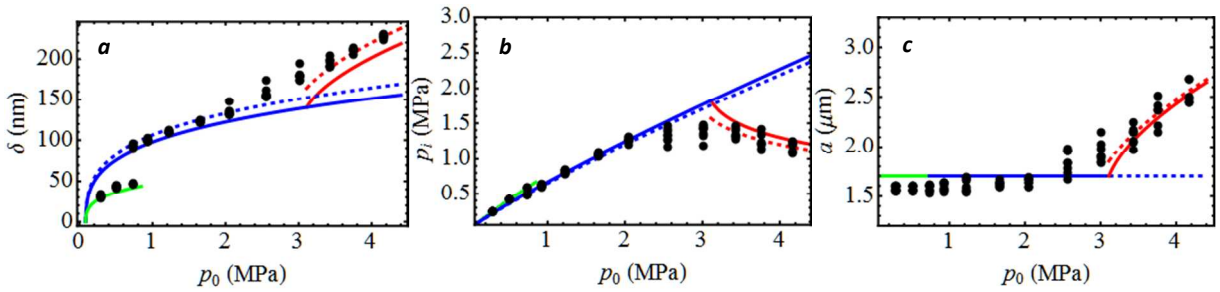

Figure 12 (a) Maximum deflection, (b) Equilibrium pressure and (c) Outer radius of the circular bulge versus the charging pressure for multi-layered graphene membranes. In each case, the green curve corresponds to the annular deformation, blue curve is for the circular deformation without delamination, and red curves are for circular deformation with delamination for different adhesion energies (dashed - C_2 =0.755, solid - C_2 =0.686).

Sliding boundary conditions can also result in symmetry breaking deformation and hence wrinkling[8]. Apparent wrinkling in varying degrees is observed in all of the multi-layered devices at higher pressures (≥ 2.56 MPa) as shown in Fig. 13.

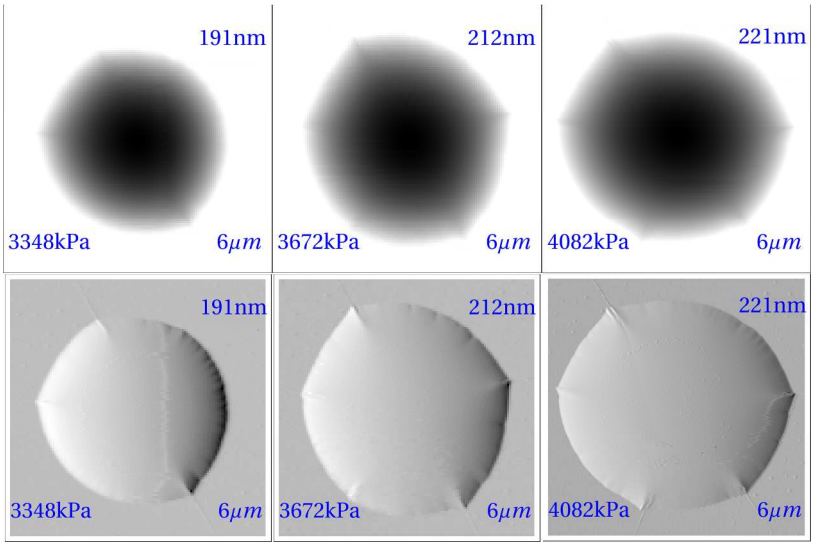

Figure 13 AFM height scans (top row) and respective derivatives (bottom row) showing wrinkling of a multi-layered device at higher pressures.

9. Adhesion Energy and Critical Charging Pressures

We obtain the adhesion energy from outward delamination using eq. (20) in combination with measured (δ, a) pairs:

$$\Gamma = \frac{5C_1}{4}\left(\frac{p_0 V_0}{V_0 + V_s(a)} - p_e\right)\delta(a) \tag{20}$$

Applying eq. (20) to all the data points which exhibit outward delamination ($a > a_0$) and averaging the adhesion energy and the blister radius at each charging pressure, we obtain the values in Table 1.

	Mono-layered Devices ($a_0 = 1.5$ μm)		Multi-layered Devices ($a_0 = 1.7$ μm)	
Charging Pressure, p_0 (MPa)	Blister Radius, a (μm)	Adhesion Energy, Γ (mJ/m^2)	Blister Radius, a (μm)	Adhesion Energy, Γ (mJ/m^2)
2.05	1.61	112.13	-	-
2.56	1.86	126.97	1.80	128.78
3.01	1.99	141.28	1.88	153.66
3.43	2.20	142.40	2.07	161.13
3.76	2.37	139.51	2.24	161.05
4.16	2.52	141.58	2.41	162.36

Table 1 Calculated adhesion energies along with the blister radii at different charging pressures

For mono-layered devices, it can be seen from Table 1 that the calculated adhesion energy increases from 112.13 mJ/m^2 at 2.05 MPa to about 140 mJ/m^2 at 3.01 MPa and then maintains at about this value at higher pressures. Likewise for multi-layered devices, the apparent adhesion energy is 128.78 mJ/m^2 at 2.56 MPa and reaches a stable value of about 160 mJ/m^2 at and above 3.43 MPa. Thus the apparent adhesion energy near the edge of the cavity is lower than that in the regions sufficiently away from the edge. This is perhaps due to topographic variations near the perimeter of the cavity (as well as near the island boundary), including a non-ideal circular boundary, a boundary that is not sharp (as assumed in our model), and roughness variations near the perimeter of the cavity. In order to estimate the critical charging pressure, p_c^o with our theory, we used the lowest apparent adhesion energy in eq. (20) with $a = a_0$ to estimate the critical charging pressure, p_c^o. This results in p_c^o = 2.0 MPa for mono-layered membranes and 2.14 MPa for multi-layered ones.

Experimentally we find that mono-layered membranes delaminate completely from the island at a charging pressure between 733 kPa and 1223 kPa. We found that two of the eight mono-layered devices remain attached to the island at 929 kPa. Based on these observations, we took 929 kPa to be our best estimate of the critical charging pressure for island delamination, p_c^i. This is because from Table 2 it is evident that the membranes are slowly delaminating from the island and at 929.0 kPa all but two of them delaminate completely. Other devices conceivably could have been still attached to the island at slightly lower charging pressures. Employing a similar argument, we assume that p_c^i is 733.0 kPa for multi-layered devices. With p_c^i = 929.0 kPa and

$b = 270.0$ nm, the adhesion energy on the island is estimated to be 102.6 mJ/m^2 for mono-layered membranes using eq. (19). It is 123.8 mJ/m^2 for multi-layered membranes with $p_c^i = 733.0$ kPa and $b = 150.0$ nm. These values are in reasonable agreement with 112.13 mJ/m^2 and 128.78 mJ/m^2, the adhesion energies near the cavity boundary obtained with the outward delamination data for mono and multi-layered membranes respectively.

Charging Pressure, p_0 (kPa)	**289.8**	**512.6**	**733.0**	**929.0**
Mono-layered Island radius, b (nm) ($b_0 = 350.0$ nm)	335.0	335.0	295.0	270.0 (2 devices)
Multi-layered Island radius , b (nm) ($b_0 = 250.0$ nm)	185.0	195.0	150.0 (3 devices)	-

Table 2 Averaged radii of the region of the membrane still attached to the island at different charging pressures

10. References

(1) Koh, Y. K.; Bae, M.-H.; Cahill, D. G.; Pop, E. *ACS Nano* **2011**, *5*, 269–74.

(2) Grabmüller, H.; Weinitschke, H. J. *J. Elast.* **1986**, *16*, 135–147.

(3) Weinitschke, H. J.; Grabmüller, H. *J. Eng. Math.* **1992**, *26*, 159–194.

(4) Saif, M. T. A.; Alaca, B. E.; Sehitoglu, H. *J. Microelectromechanical Syst.* **1999**, *8*, 335–345.

(5) Williams, J. G. *Int. J. Fract.* **1997**, *87*, 265–288.

(6) Hencky, H. *Z. Math. Phys.* **1915**, *63*, 311–317.

(7) Kitt, A.; Qi, Z.; Remi, S.; Park, H. S.; Swan, A. K.; Goldberg, B. *Nano Lett.* **2013**, 130429083808009.

(8) Cheo, L. S.; Reiss, E. L. *Q. Appl. Math.* **1973**, *31*, 75–91.